AIP | Applied Physics Letters

Defect-free ZnO nanorods for low temperature hydrogen sensor applications

Sapana Ranwa, Pawan K. Kulriya, Vikas Kumar Sahu, L. M. Kukreja, and Mahesh Kumar

Citation: Applied Physics Letters **105**, 213103 (2014); doi: 10.1063/1.4902520
View online: http://dx.doi.org/10.1063/1.4902520
View Table of Contents: http://scitation.aip.org/content/aip/journal/apl/105/21?ver=pdfcov
Published by the AIP Publishing

Defect-free ZnO nanorods for low temperature hydrogen sensor applications

Sapana Ranwa,[1] Pawan K. Kulriya,[2] Vikas Kumar Sahu,[3] L. M. Kukreja,[3] and Mahesh Kumar[1,a)]
[1]*Centre for Information and Communication Technology, Indian Institute of Technology Jodhpur, Jodhpur 342011, India*
[2]*Inter University Accelerator Centre, Aruna Asaf Ali Marg, New Delhi 110067, India*
[3]*Laser Materials Processing Division, Raja Ramanna Centre for Advanced Technology, Indore 452 013, India*

(Received 13 October 2014; accepted 13 November 2014; published online 24 November 2014)

Uniformly distributed and defect-free vertically aligned ZnO nanorods (NRs) with high aspect ratio are deposited on Si by sputtering technique. X-ray diffraction along with transmission electron microscopy studies confirmed the single crystalline wurtzite structure of ZnO. Absence of wide band emission in photoluminescence spectra showed defect-free growth of ZnO NRs which was further conformed by diamagnetic behavior of the NRs. H_2 sensing mechanism based on the change in physical dimension of channel is proposed to explain the fast response (~21.6 s) and recovery times (~27 s) of ZnO NRs/Si/ZnO NRs sensors. Proposed H_2 sensor operates at low temperature (~70 °C) unlike the existing high temperature (>150 °C) sensors. © *2014 AIP Publishing LLC*. [http://dx.doi.org/10.1063/1.4902520]

Metal oxide semiconductor materials are commonly used for various sensing applications.[1] ZnO is a most versatile among all metal oxide semiconductors, due to its wide direct band gap (~3.24 eV), high excitation binding energy (~60 meV), high thermal and chemical stability, and unique electrical and optical properties.[2] Gas sensors based on low-dimension structures[3–5] are more suitable than thin film based gas sensors[6] because of large aspect ratio and small dimension helps in quantum confinement of charge. Nanostructures provide the large surface area for chemical reactions than thin films which enhance recovery and response times at low operating temperature.[7] ZnO thin films or nanostructures based gas sensors sensitivity mainly depends on crystallinity, grain size, operating temperature, and aspect ratio.[8] ZnO nanostructures are used in various sensing applications such as humidity sensor,[9] SAW devices,[10] chemical sensor,[11] and bio sensor.[12] Hydrogen (H_2) is most widely used as clean energy source in fuel cells and hydrogen engines. At present, available H_2 sensors are operating at higher temperature that is above 150 °C. Due to highly explosive nature of H_2 at high temperature, low ignition energy, and its non-adorable nature demands to develop H_2 sensors with low operating temperature. Schottky barrier height is highly influenced by adsorption/desorption of oxygen, which enhance the sensitivity of the devices.[13] Wei *et al.*[14] explain that schottky barrier height amplifies surface chemisorbed gases and increases sensitivity four times higher than ohmic junction. ZnO nanowires exhibited higher H_2 sensitivity than conventional ZnO thin film at elevated temperature (200 °C).[15] Wang *et al.*[16] fabricated Zn doped NiO dendritic crystal with nano-tree and reported fast response and self-recovery for ammonia detection at room temperature. ZnO nanowires fabricated using ultra-fast microwave synthesis process showed high sensitivity with fast response time (65 s) on exposure to H_2 gas having concentration about 500 ppm in air.[17] Hassan *et al.*[18] reported flexible metal/ZnO NRs/metal devices having maximum sensitivity up to 150% for 2% H_2 in N_2 at operating temperature 200 °C. In the present work, the hydrogen sensing characteristic of the ZnO NRs/Si/ZnO NRs double Schottky junctions is reported.

Vertically aligned, uniformly distributed ZnO nanorods (NRs) were deposited on n-Si(100) wafer using RF-sputtering technique. Silicon wafer was chemically cleaned followed by HF dip (5%) which removed native oxide from the substrate. ZnO target (99.999% purity) was used for NRs deposition in presence of pure argon (99.999% purity). During deposition, chamber pressure and substrate temperature were maintained at 2×10^{-2} mbar and 500 °C, respectively, with a constant Ar gas flow of 60 sccm. RF power was maintained at 150 W and target to substrate distance around ~14 cm. Deposition time was kept 2 h. Structural characterizations were carried out using XRD and TEM. Surface morphologies and optical characterization were studied using field emission scanning electron microscope (FESEM) and photoluminescence (PL) spectra. Magnetic properties were studied at room temperature using Vibrating Sample Magnetometer (VSM). Au (200 nm)/Ti (20 nm) metal contact on ZnO NRs and Al (200 nm) on Si of 500 nm diameters were deposited by thermal evaporation using physical mask. ZnO NRs/n-Si/ZnO NRs devices were fabricated by selective wet chemical etching. For H_2 gas, sensing measurements were performed in vacuum chamber with 2×10^{-3} mbar chamber pressure. ZnO nanorods/n-Si/ZnO NRs device was heated up at a constant temperature of 70 °C and gas flow was controlled using mass flow controller. Resistivity with respect to time was measured using Aglient (B2911A) source meter.

FESEM images [Figs. 1(a) and 1(b)] show top view and cross-section view of ZnO NRs, respectively. From the figure, it can be seen that NRs are self-aligned with circular diameter spread over the entire substrate. The calculated value of height, diameter, density, and aspect ratio of ZnO NRs are ~750 nm, 48 nm, 1.26×10^{10} cm^{-2}, and 15.62, respectively. The ZnO NRs were removed from substrate by sonication in acetone and placed on TEM grids. TEM image and selected

a)Author to whom correspondence should be addressed. Electronic mail: mkumar@iitj.ac.in

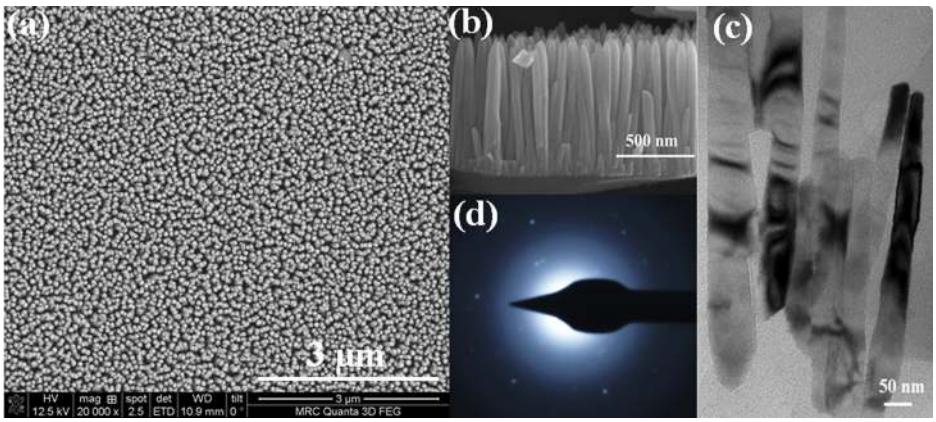

FIG. 1. (a) Top view, (b) cross-sectional view of FESEM images of ZnO NRs, (c) TEM image, and (d) SEAD pattern of ZnO NR.

area electron diffraction (SEAD) pattern are shown in Figs. 1(c) and 1(d). The diameter and heights of NRs in TEM images are very close to FESEM results. In SEAD pattern, the presence of only bright spots conform the single crystalline nature of ZnO.[19] The 2θ-ω scan of XRD patterns [Fig. 2(a)] showing a strong peak at peak position of $2\theta = 34.64°$ with FWHM ~12 arc min corresponding to (0002) diffraction of wurtzite ZnO. X-ray results clearly indicate that the NRs are grown along vertical [0002] direction.[20] Room temperature PL spectra are shown in Fig. 2(b), and it shows a sharp peak around ~3.26 eV with FWHM 130 meV indexed near band emissions (NBEs) transitions.

Normally, a broad band emission peak in PL spectra at room temperature is observed due to the presence of structural defects.[21] Absence of broad band emission region in the PL spectra clearly indicates that the ZnO NRs are grown with defect-free. Further, this is verified by VSM study. Fig. 2(c) shows magnetization versus magnetic field (M-H) curve for ZnO NRs/n-Si and bare n-Si. After subtracting substrate contribution, ZnO NRs show diamagnetic behavior and is shown in Fig. 2(d). Ferromagnetism is observed in ZnO nanostructures due to presence of oxygen vacancy defects.[22] The high temperature annealing performed on ZnO NRs in presence of oxygen showed ferromagnetic to diamagnetic behavior due to removal of oxygen vacancy defects.[23] Thus, the absence of ferromagnetism confirm the growth of defect free NRs, which is also supported by PL results.

The schematic diagram of ZnO NRs/n-Si single heterojunction (SHJ) and ZnO NRs/n-Si/ZnO NRs double heterojunctions (DHJs) are shown in the inset of Fig. 3(a). Fig. 3(a) shows current density versus voltage (J-V) characteristics of SHJ and DHJs at room temperature. The observance of rectifying behavior in J-V curve of SHJ indicates the presence of schottky barrier at junction and the calculated value of rectification ratio was ~5.7 at 3 V with leakage current density 2.53 A/cm^2. DHJs give symmetric characteristic of J-V in forward and reverse bias due to symmetry in the device structure. Ideality factor (η) and barrier height (ϕ_B) of the

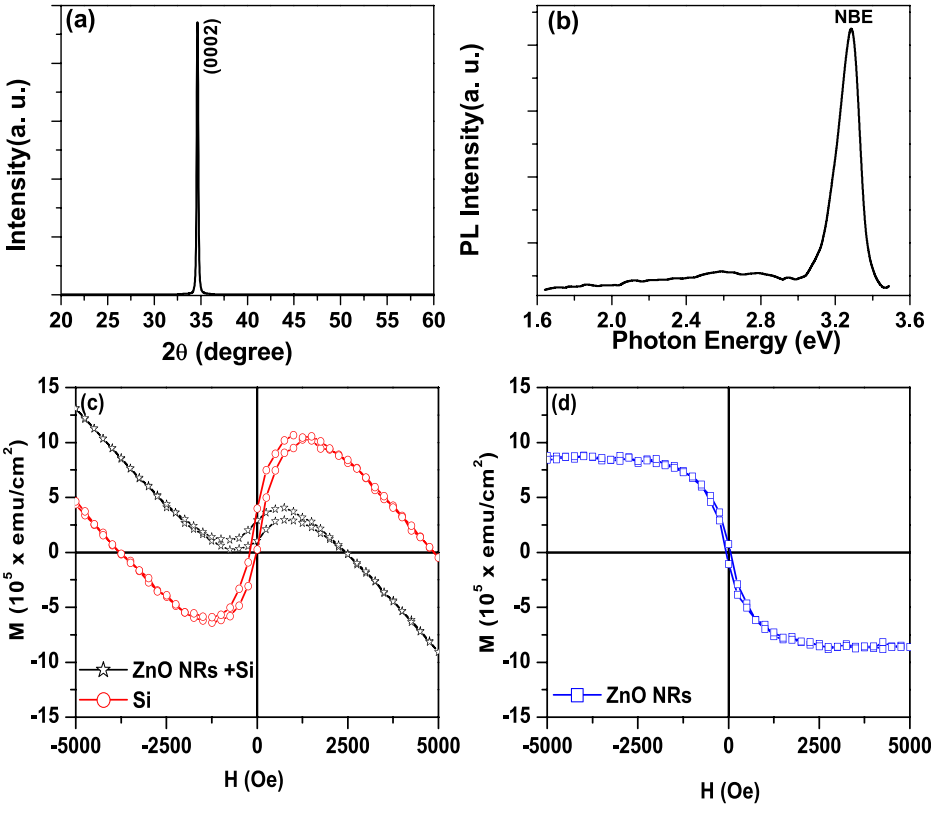

FIG. 2. (a) X-Ray diffraction 2θ-ω scan, (b) room temperature PL spectra, and magnetization versus magnetic field (M-H) curve for (c) ZnO NRs/Si and bare Si, and (d) for ZnO NRs.

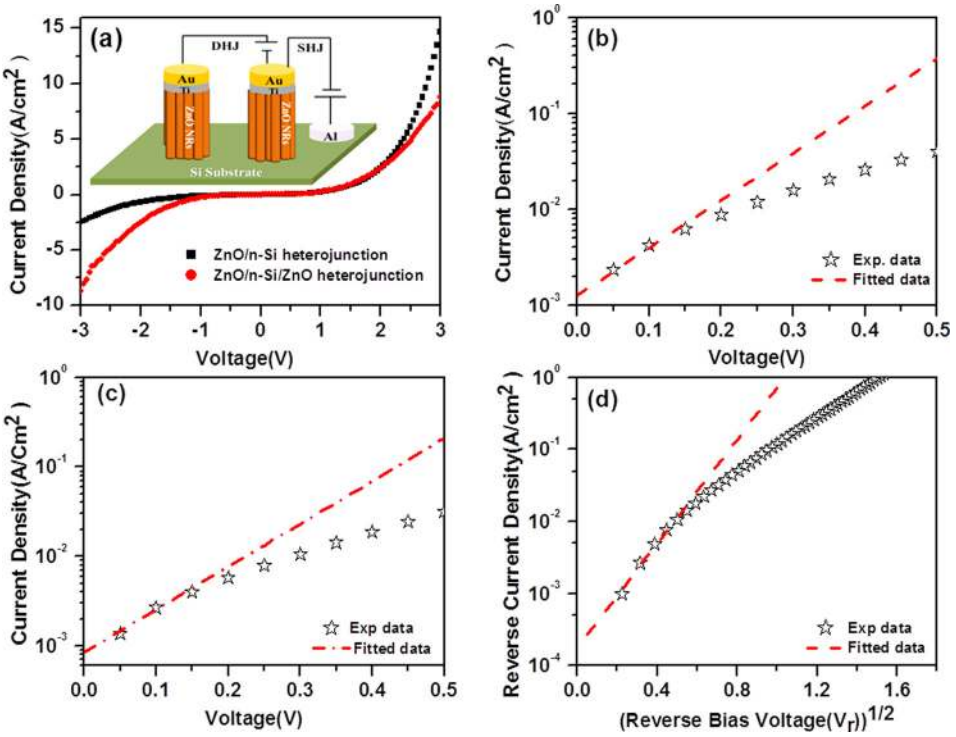

FIG. 3. (a) Room temperature *J-V* characterization for ZnO NRs/Si SHJ and ZnO NRs/Si/ZnO NRs DHJs, (b) and (c) show linear fitting of forward bias region for SHJs and DHJs, respectively, and (d) shows schottky barrier height of reverse bias of SHJs. Schematic diagram of devices contacts, ZnO NRs/Si SHJ and ZnO NRs/Si/ZnO NRs DHJs are shown in inset.

SHJ and DHJs were calculated by using thermionic emission model by fitting for linear region of current density in forward bias. Current density of these two heterojunction is given by[24]

$$J = J_o\left\{\exp\left(\frac{qV}{\eta kT}\right) - 1\right\}, \tag{1}$$

where J_o is reverse saturation current density given by

$$J_o = A^* T^2 \exp\left(\frac{-q\phi_B}{kT}\right). \tag{2}$$

Here T, ϕ_B, k, A^*, and η are operating temperature, barrier height, Boltzmann constant, Richardson constant ($112\,\mathrm{A\,cm^{-2}K^{-2}}$ for n-Si), and Ideality factor, respectively. Figs. 3(b) and 3(c) show linear region fitting in forward bias. Barrier height and ideality factor are calculated by thermionic emission model and found to be $\phi_B = 0.59\,\mathrm{eV}$ and $\eta = 3.4$ for SHJ and $\phi_B = 0.60\,\mathrm{eV}$ and $\eta = 3.5$ for DHJs. Schottky barrier height of reverse bias of SHJ is also calculated using Bardeen model[25] and shown in Fig. 3(d). Rakhshani *et al.*[26] explained the Bardeen model as linearly decay of barrier height when electric field increases. This model gives relation between reverse saturation current density at SHJ with respect to square root of applied reverse biased voltage as below

$$J = J_r \exp\left(\frac{\beta\sqrt{V_r}}{kT}\right), \tag{3}$$

where β is interface related parameter and J_r is given as reverse saturation current density calculated as

$$J_r = A^* T^2 \exp\left(\frac{-q\phi_r}{kT}\right). \tag{4}$$

Exponential fitting were used to calculate reverse barrier height (ϕ_r) as given in Eq. (3)

$$J = a\exp\left(b\sqrt{V}\right), \tag{5}$$

where a is defined as J_r which used to calculate reverse schottky barrier height. Reverse barrier height of SHJ was found to be $\sim\phi_r = 0.62\,\mathrm{eV}$. Schottky barrier height is highly influenced by adsorbed/desorption of oxygen which enhances the sensitivity of the device.[13,14] The DHJs would play an important role to enhance H_2 sensitivity and similarly, ZnO NRs/Si/ZnO NRs double schottky junctions are fabricated.

Hydrogen gas sensing properties of ZnO NRs were measured at a pressure of about $2\times10^{-3}\,\mathrm{mbar}$. Hydrogen sensing for ZnO depends on adsorption and desorption of environmental oxygen to form depletion region on NRs. When ZnO nanorods reacts with environmental oxygen and gases, its sensitivity towards gases changes and it depends upon adsorbed oxygen (O^-, O^{2-}, O_2^-) ions and defects. Initially, when ZnO NRs are exposed to air, oxygen is adsorbed on surface of nanorods which lead to extraction of electron from the conducting region of NRs and forms depletion region. Due to depletion region formation in NRs, its conduction channel area decreases which result in decrease in the conduction of the device. Electrical conduction (G) of ZnO NRs strongly dependent on number of conducting electrons as given by the following equation:[27]

$$G = \frac{1}{R} = \frac{n|e|\mu\pi r^2}{l}, \tag{6}$$

where n, e, r, μ, and l are charge carrier concentration, electron charge, radius of NR, electron mobility, and length of NR, respectively. Since gas sensitivity is directly proportional to conduction cross-section channel area of NRs.

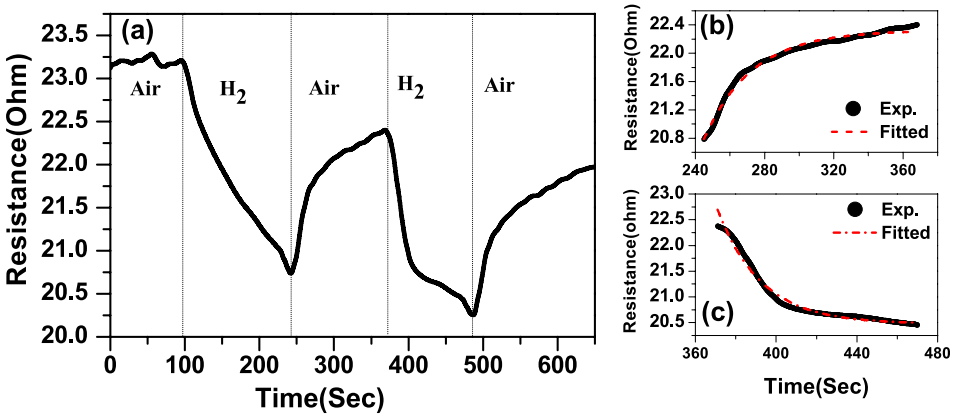

FIG. 4. (a) Resistivity response of ZnO NRs/Si/ZnO NRs device at 70 °C and (b) and (c) show exponential fitting of resistivity response curve for recovery and response time, respectively.

Therefore, channel area changes as depletion channel width changes. At the time of hydrogen loading, negative oxygen ion react with H_2 and forms H_2O as well as release electron in to the layer. Thus, desorption of oxygen transfer the electrons into NRs, which leads to increases in the channel cross-section area and decrease in resistance. Sensitivity of gas sensor is defined as ratio of change in resistance in air with respect to H_2 gas.[28] In this study, ZnO NRs/n-Si/ZnO NRs double schottky junction were used for hydrogen detection at relatively low operating temperature. Resistive response of ZnO NRs/n-Si/ZnO NRs were measured at 70 °C in H_2 environment and shown in Fig. 4(a). The variation in the minimum value of resistance in case of first and second cycle is ~2.5%, whereas for other cycles is ~±0.5%. The charges (O^{2-} ions) on the surface of ZnO NRs are not completely released in the first cycle, while in second cycle it removes most of the O^{2-} ions and changes the minimum value of resistance. Also there is possibility that some hydrogen atoms are trapped in the NRs in first cycle and dimension of the NR itself might be changed due to swelling in the NR.[29] As a consequence, the dimension of NRs also increases which decreases the resistance in second cycle. Response time, recovery time, and sensitivity are three key parameters for any gas sensor. The response time or decay time (τ_d) which represented as change in 90% of saturation resistance with loading of hydrogen, while deloading of hydrogen gas through chamber shows exponentially increase in resistance response gives recovery or rise time (τ_r). Figs. 4(b) and 4(c) show the decay and rise time exponential fitting of following equations:[30]

$$R = R_0 + A\exp\left(\frac{t}{\tau_r}\right), \tag{7}$$

$$R = R_1 + B\exp\left(-\frac{t}{\tau_d}\right), \tag{8}$$

where A and B are scaling constant. From these fitting, rise and decay time constant were calculated as 27 s and 21.6 s, respectively, which shows fast response and recovery time at relatively low operating temperature.[17,18,31] Tien *et al.*[32] reported three times higher response time for ZnO NRs in comparison to ZnO thin film. Sensitivity (relative change in resistance) of ZnO NRs/n-Si/ZnO NRs sensor was found to be ~10.05% in the presence of pure hydrogen. There are many reports on ZnO nanostructure based hydrogen sensor with high sensitivity but operating temperature was kept above 150 °C.[15,17] Al-Salman and Abdullah[33] reported ZnO nanostructure based H_2 sensor having high defect density and operated at 200 °C which shows high sensitivity. In this study, ZnO NRs are defect free and showed high sensitivity for H_2 gas at low operating temperature.

Based on experimental observation a gas sensing mechanism is proposed and shown in Fig. 5. Chemisorbed oxygen ions totally depend on temperature of operation. At lower temperature, O^{2-} ions are dominantly adsorbed by NRs but at higher temperature (>150 °C) these ion are negligible and O^{-} ions are dominantly adsorbed. When NRs interact with oxygen, form a depletion region and decreases resultant

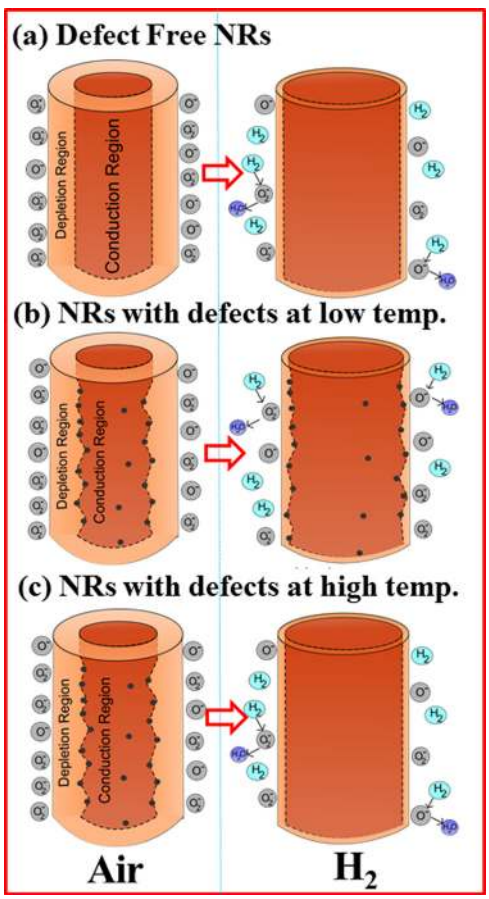

FIG. 5. (a)–(c) Show schematic diagram of gas sensing mechanism of defect free ZnO NRs, defect contained ZnO NRs at low and high (>150 °C) operating temperatures, respectively.

channel diameter of conduction. During the loading of H_2 reacts with oxygen ion and increase channel diameter and as a result the channel resistance decreases.[34] Figs. 5(a)–5(c) show schematic diagram of gas sensing mechanism of defect free ZnO NRs, defect contained ZnO NRs at low and high (>150 °C) operating temperatures, respectively. Due to presence of defects at low temperature, hydrogen reaction on NRs increases channel diameter but its lesser compared to high temperature operation as shown in Fig. 5. Since higher energy or temperature is required to completely remove the adsorbed oxygen from defect points.[35] Thus, we can say that gas sensitivity could be higher in the presence of defects at high operating temperature (>150 °C) due to larger conduction region. However, at low operating temperature sensitivity could be lower in the presence of defects in NRs. In this study, ZnO NRs are grown with defects-free which show high sensitivity at low temperature. Hence, defect free low dimensional structures can be used at low temperature for hydrogen gas sensor.

In conclusion, vertically aligned defect free ZnO NRs were grown on Si substrate. The hexagonal wurtzite structure of ZnO nanorods was confirmed using XRD and TEM. FESEM image shows that NRs are uniformly grown on the substrate. PL gives a strong peak around ~380 nm indicates optical band gap around 3.26 eV. Absence of wide band emission bands indicate defects free growth of ZnO NRs. Room temperature VSM also gives diamagnetic behavior due to absent of oxygen defects in ZNO NRs. ZnO NRs/n-Si/ZnO NRs double schottky junction were used as sensor for hydrogen gas. Double Schottky junction enhances sensitivity of the device. The device is found to have fast response (~21.6 s) and recovery time (~27 s) during loading/deloading of pure hydrogen at 100 mbar gas pressure because of high aspect ratio and uniformity of nanorods. This sensor setup gives sensitivity $S \sim 10.05\%$ at the operating temperature of 70 °C. This presents a mechanism to fabricate hydrogen sensors, which can operate at low temperature unlike the existing hydrogen sensors, which operate at high temperature. By changing NRs aspect ratio and with transition metals or rare earth element doping gas sensitivity can be enhanced in future. Based on experimental results, a H_2 gas sensing mechanism is proposed for defect-free NRs.

The authors acknowledge the financial support from Department of Atomic Energy (DAE) Project No. 34/14/16/2014-BRNS with ATC and the help of Jitendra Singh, CEERI Pilani for the VSM measurements. Authors would also like to acknowledge Dr. Satyajit Sahu for discussion.

[1]C. C. Li, Z. F. Du, L. M. Li, H. C. Yu, Q. Wan, and T. H. Wang, Appl. Phys. Lett. **91**, 032101 (2007).
[2]Z. Fan and J. G. Lu, J. Nanosci. Nanotechnol. **5**, 1561 (2005).
[3]C. Wang, X. Chu, and M. Wu, Sens. Actuators, B **113**, 320 (2006).
[4]M. Kashif, M. E. Ali, S. M. U. Ali, U. Hashim, and S. B. A. Hamid, Nano. Res. Lett. **8**, 68 (2013).
[5]X. Sun, L. Qiao, and X. Wang, Nano-Micro. Lett. **5**, 191 (2013).
[6]Q. G. Al-Zaidi, A. M. Suhail, and W. R. Al-Azawi, Appl. Phys. Res. **3**, 89 (2011).
[7]Z. H. Lim, Z. X. Chia, M. Kevin, A. S. W. Wong, and G. W. Ho, Sens. Actuators, B **151**, 121 (2010).
[8]V. Bochenkov and G. Sergeev, Adv. Colloid Interface Sci. **116**, 245 (2005).
[9]L. Chen and J. Zhang, Sens. Actuators, A **178**, 88 (2012).
[10]H. S. Hong, D. T. Phan, and G. S. Chung, Sens. Actuators, B **171–172**, 1283 (2012).
[11]R. Ahmad, N. Tripathy, D. U. J. Jung, and Y. B. Hahn, Chem. Commun. **50**, 1890 (2014).
[12]M. Q. Israr, J. R. Sadaf, O. Nur, M. Willander, S. Salman, and B. Danielsson, Appl. Phys. Lett. **98**, 253705 (2011).
[13]M. Shafiei, J. Yu, R. Arsat, K. K. Zadeh, E. Comini, M. Ferroni, G. Sberveglieri, and W. Wlodarski, Sens. Actuators, B **146**, 507 (2010).
[14]T. Y. Wei, P. H. Yeh, S. Y. Lu, and Z. L. Wang, J. Am. Chem. Soc. **131**, 17690 (2009).
[15]N. L. Hung, E. Ahn, S. Park, H. Jung, H. Kim, S. K. Hong, D. Kim, and C. Hwang, J. Vac. Sci. Technol., A **27**, 1347 (2009).
[16]J. Wang, L. Wei, L. Zhang, J. Zhang, H. Wei, C. H. Jiang, and Y. F. Zhang, J. Mater. Chem. **22**, 20038 (2012).
[17]A. Qurashi, N. Tabet, M. Faiz, and T. Yamzaki, Nano. Res. Lett. **4**, 948 (2009).
[18]J. J. Hassan, M. A. Mahdi, S. J. Kasim, N. M. Ahmed, H. A. Hassan, and Z. Hassan, Mater. Sci.-Pol. **31**, 180 (2013).
[19]X. Xu, C. Xu, Y. Lin, T. Ding, S. Fang, Z. Shi, W. Xia, and J. Hu, Appl. Phys. Lett. **100**, 172401 (2012).
[20]S. Ranwa, P. K. Kulriya, V. Dixit, and M. Kumar, J. Appl. Phys. **115**, 233706 (2014).
[21]C. Chandrinou, N. Boukos, C. Stogiou, and A. Travlos, Microelectron. J. **40**, 296 (2009).
[22]A. Sundaresan, R. Bhargavi, N. Rangarajan, U. Siddesh, and C. N. R. Rao, Phys. Rev. B **74**, 161306 (2006).
[23]B. Panigrahy, M. Aslam, D. S. Misra, M. Ghosh, and D. Bahadur, Adv. Funct. Mater. **20**, 1161 (2010).
[24]B. Roul, M. K. Rajpalke, T. N. Bhat, M. Kumar, N. Sinha, A. T. Kalghatgi, and S. B. Krupanidhi, J. Appl. Phys. **109**, 044502 (2011).
[25]J. Zhang and W. R. Harrell, J. Vac. Sci. Technol., B **21**, 872 (2003).
[26]A. E. Rakhshani, Y. Makdisi, X. Mathew, and N. Mathews, Phys. Status Solidi A **168**, 177 (1998).
[27]O. Lupan, V. V. Ursaki, G. Chai, L. Chow, G. A. Emelchenko, I. M. Tiginyanu, A. N. Gruzintsev, and A. N. Redkin, Sens. Actuators, B **144**, 56 (2010).
[28]H. Gu, Z. Wang, and Y. Hu, Sensors **12**, 5517 (2012).
[29]F. Favier, E. C. Walter, M. P. Zach, T. Benter, and R. M. Penner, Science **293**, 2227 (2001).
[30]A. Z. Adamyan, Z. N. Adamyan, V. M. Aroutiounian, K. D. Schierbaum, and S. D. Han, Armenian J. Phys. **2**, 200 (2009), available at http://ajp.asj-oa.am/180/1/06.Adamyan.pdf.
[31]C. S. Rout, S. Hari Krishna, S. Vivekchand, A. Govindaraj, and C. Rao, Chem. Phys. Lett. **418**, 586 (2006).
[32]L. C. Tien, P. W. Sadik, D. P. Norton, L. F. Voss, S. J. Pearton, H. T. Wang, B. S. Kang, F. Ren, J. Jun, and J. Lin, Appl. Phys. Lett. **87**, 222106 (2005).
[33]H. S. Al-Salman and M. J. Abdullah, Sens. Actuators, B **181**, 259 (2013).
[34]C. L. Hsu, Y. D. Gao, Y. S. Chen, and T. J. Hsueh, Sens. Actuators, B **192**, 550 (2014).
[35]H. Nan, Z. Wang, W. Wang, Z. Liang, Y. Lu, Q. Chen, D. He, P. H. Tan, F. Miao, X. Wang, J. Wang, and Z. Ni, ACS Nano **8**, 5738 (2014).